Rheology of granular suspensions
Shearing flows of granular suspension

Élisabeth Guazzelli

Université de Paris, CNRS, Matière et Systèmes Complexes (MSC)

from Chapter 7 of *A Physical Introduction to Suspension Dynamics* CUP 2012
by É. Guazzelli & J. F. Morris (illustrations by S. Pic)

and from *Rheology of dense granular suspensions* JFM Perspective 2018
by É. Guazzelli & O. Pouliquen

Collective behavior of particles in fluids
IHP Paris, December 14-17, 2020

Complex mobile particulate systems

used in engineering and found in nature

self-compacting concrete
https://www.youtube.com/watch?v=owKLhrv7Zbk

heavy rain from ex-cyclone Gita turns Rakaia river into a river of rock
https://www.youtube.com/watch?v=5AwFSSX34Wo

$\rightarrow$ **understanding the rheology of suspensions**

Model suspensions

Aussillous, Chauchat, Pailha, Medale & Guazzelli JFM 2013

$\rightarrow$ understanding the rheology of model suspensions . . .
and moving toward more complex mixtures of particles and fluids

"A major difficulty in the study of rheology is that one's intuition about the form of the constitutive stress relation appropriate to given circumstances is so poorly developed. It is often hard to know even in broad terms how a given material will behave, chiefly because we have at our disposal so few definite and well-understood constitutive relations for non-Newtonian fluids to provide guidance. This difficulty affects mathematical theory as well as the interpretation of observation, since, for lack of concrete results which can be used as a testing ground, the hypotheses on which analysis must perforce be based tend to be artificial and unmotivated. Now the microscopic structure of a suspension can be precisely specified, and it may be possible–and not only in principle–to *deduce* some of the macroscopic properties of the suspension and to see in explicit terms their relation to the microstructure. This seems to me **to give the mechanics of suspensions an especially important place in current studies of rheology**, in that we have the **unusual opportunity of obtaining definite and explicable constitutive relations** which are known to apply to specifiable materials and which may be used as a reliable guide for intuition."

Batchelor JFM 1970 *The stress system in a suspension of force-free particles*

The different regimes

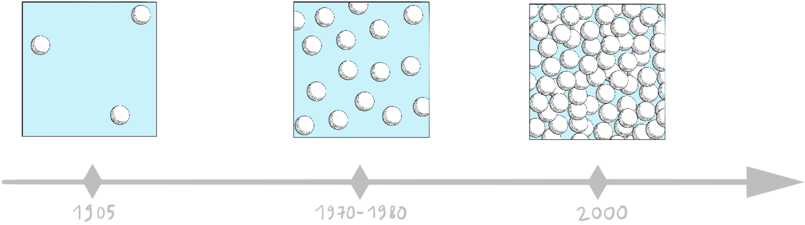

Dilute

Single particle

Semi-dilute

Hydrodynamic interactions

Concentrated

Contact interactions

A sheared viscous suspension of non colloidal particles

Suspension of neutrally-buoyant hard spheres

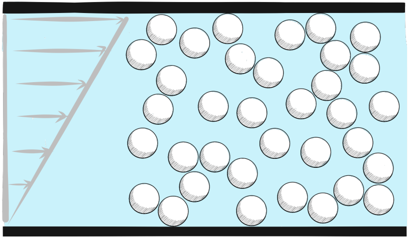

Buoyancy effect

$$\frac{\rho_p - \rho_f}{\rho_f} \to 0$$

Inertial/viscous effects

$$Re_p = \frac{\rho_f a^2 \dot{\gamma}}{\eta_f} \to 0$$

Brownian motion

$$Pe = \frac{6\pi\eta_f \dot{\gamma} a^3}{kT} \to \infty$$

Suspension viscosity

Suspension of rigid, neutrally-buoyant, non-colloidal, mono-disperse, hard spheres

The scaling of the shear stress is viscous: $\tau = \eta_s(\phi)\,\eta_f\dot{\gamma}$ with $\dot{\gamma} = \sqrt{2\,\mathbf{E}:\mathbf{E}}$

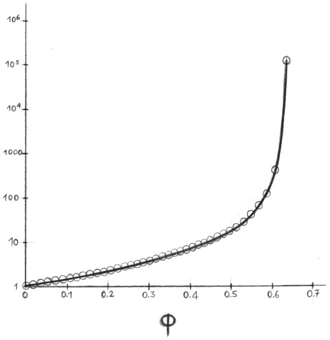

from *A Physical Introduction to Suspension Dynamics*
Guazzelli & Morris (Illustrations by Pic)
Cambridge Texts in Applied Mathematics CUP 2012

Viscosity $O(\phi)$

Einstein Ann. Phys. 1906, 1911

$\eta_s = 1 + 5\phi/2$

First effect of particle pair interactions $O(\phi^2)$

Batchelor & Green JFM 1972

$\eta_s = 1 + \frac{5}{2}\phi + k\phi^2$ with $k \approx 5$

Hydrodynamic interactions

Brady & Bossis ARFM 1988; Nott & Brady JFM 1994 ...

Stokesian dynamics; constitutive laws

Jamming transition

Lerner *et al.* PNAS 2012; Andreotti *et al.* PRL 2012 ...

Extended network of contacts at jamming : steric/elastic interactions

The averaging process for a suspension

Bulk stress

Ensemble average of the stress distribution in all realizations of the suspension

Statistically homogeneous suspension

Ensemble average $\equiv$ volume average

$$
\begin{aligned}
\Sigma_{ij} &= \langle \sigma_{ij} \rangle \\
&= \frac{1}{V} \int_V \sigma_{ij} dV \\
&= \frac{1}{V} \int_{V_f} \sigma_{ij} dV + \frac{1}{V} \int_{V_p} \sigma_{ij} dV
\end{aligned}
$$

Landau & Lifshitz 1959; Batchelor JFM 1970

Particle contribution to the bulk stress

Bulk stress

$$\boldsymbol{\Sigma} = -\langle p \rangle \mathbf{I} + 2\eta_f \langle \mathbf{e} \rangle + \boldsymbol{\Sigma}^{(p)}$$

Particle contribution

$$\Sigma_{ij}^{(p)} = \frac{1}{V} \int_{S_p} [\sigma_{ik} x_j - \frac{1}{3} \delta_{ij} \sigma_{lk} x_l] n_k \, dS = n \langle S_{ij} \rangle$$

- Symmetric part (- trace) = stresslet

$$S_{ij} = \frac{1}{2} \int_{S_p} (\sigma_{ik} x_j + \sigma_{jk} x_i - \frac{2}{3} \delta_{ij} \sigma_{lk} x_l) n_k \, dS \quad \textbf{for rigid particles with no external forces}$$

- Antisymmetric part = couplet → torque[a]

$$A_{ij} = \frac{1}{2} \int_{S_p} (\sigma_{ik} x_j - \sigma_{jk} x_i) n_k \, dS \equiv -\frac{1}{2} \epsilon_{ijk} T_k$$

[a] $-\epsilon_{ijk} A_{jk} = -\epsilon_{ijk} \int_{S_p} (\boldsymbol{\sigma} \cdot \mathbf{n})_j \, x_k \, dS = T_i$

Single solid sphere in a shear

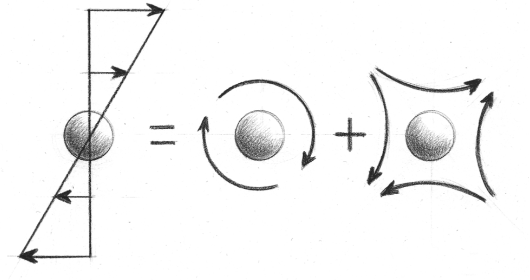

NO force and NO torque BUT stresslet $\mathbf{S} = \frac{20\pi}{3}\eta_f a^3 \mathbf{E}^\infty$

Result of the resistance of the rigid particle to the straining motion

Einstein viscosity

One solid sphere freely suspended (force-free and torque-free)

$$\rightarrow \quad \text{stresslet} \quad \mathbf{S^h} = \frac{20}{3}\pi\eta_f a^3 \langle \mathbf{e} \rangle$$

Bulk stress of a dilute suspension of solid spheres at $O(\phi)$

$$\begin{aligned} \mathbf{\Sigma} &= -\langle p \rangle \mathbf{I} + 2\eta_f \langle \mathbf{e} \rangle + n\frac{20}{3}\pi\eta_f a^3 \langle \mathbf{e} \rangle \\ &= -\langle p \rangle \mathbf{I} + 2\eta_f (1 + \frac{5}{2}\phi) \langle \mathbf{e} \rangle \quad \text{with} \quad \phi = \frac{4}{3}\pi a^3 n \end{aligned}$$

Einstein effective viscosity

$$\eta_E = 1 + \frac{5}{2}\phi$$

Einstein Ann. Phys. 1906, 1911

A pair of spheres in a shear flow

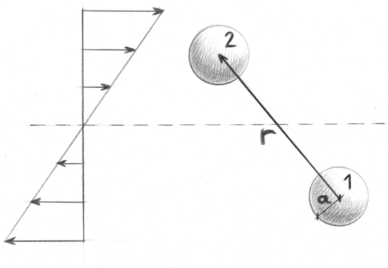

Summing the effects between pairs of particles

- Method of reflections:
  - Flow due to the stresslet of particle 2 at particle 1: $\mathbf{u}_2^0 \sim O(r^{-2})$
  - Rate of strain at particle 1 due to particle 2: $\mathbf{e}_2^0 \sim \nabla \mathbf{u}_2^0 \sim O(r^{-3})$
  - Incremental stresslet due to a second particle: $\boldsymbol{\Delta}\mathbf{S}(\mathbf{r}) \sim O(r^{-3})$
- Averaging over all possible separations which occur with conditional pair probability $P_{1|1}(r)$

$$n\langle \mathbf{S} \rangle = n\mathbf{S}_0 + n \int_{r \geq 2a} \boldsymbol{\Delta}\mathbf{S} \; \underbrace{P_{1|1}(r)}_{ng(r)\approx n}(\mathbf{r})\, dV$$

- Non-convergent integral due to **long-range hydrodynamic interactions**

$$n \int_{r \geq 2a} \boldsymbol{\Delta}\mathbf{S}\; P_{1|1}(\mathbf{r})\, dV \sim n^2 \int_{2a}^{L} r^{-3} r^2 dr \sim n^2 \ln L$$

Effective viscosity at $O(\phi^2)$

Need renormalization of hydrodynamic interactions

$$\eta_s = 1 + \frac{5}{2}\phi + k\phi^2$$

- For pure straining, by trajectory calculation of nonuniform probability distribution of separation of pairs

$$k = 6.95\,(\approx 7.6 \pm 0.8)$$

- For pure shear, problem of closed trajectories (depends on distribution on closed orbits)

$$k \approx 5$$

- For strong Brownian motion (suspension of hard spheres at uniform equilibrium + Brownian contribution coming from pair distribution function out off equilibrium)

$$k = 6.2\,(= 5.2 + 0.99)$$

Batchelor & Green JFM 1972, Batchelor JFM 1977

Stokes-flow trajectories of 2 spheres in simple shear

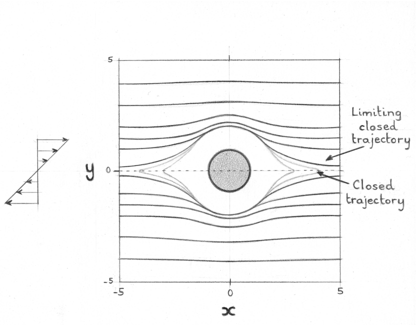

Batchelor & Green JFM 1972

- Motion exhibits fore-aft symmetry
- Presence of closed trajectories
- Compression of particle trajectories near contact
  ∴ close approach and bundling of trajectories

Reversible trajectories extremely sensitive to near-contact perturbations!

See also Irreversibility

Viscosity for larger ϕ

Computing the viscosity for larger ϕ is very difficult as multi-body hydrodynamic interactions must be computed together with determining the microstructure. Another complexity is that the spheres can interact not only by hydrodynamic interactions through the liquid but also by direct mechanical contact.

- NO exact analytic calculations
- Simulations with various levels of approximation and sophistication: from Stokesian dynamics to lattice-Boltzmann or fictitious domains methods

Empirical relations

Some of these expressions stem from mean-field approaches. They recover the Einstein viscosity limit at low concentration and aim to account for the divergence of the viscosity at ϕ_c:

- $\eta_s/\eta = (1 - \frac{\phi}{\phi_c})^{-\frac{5}{2}\phi_c}$ (Krieger)
- $\eta_s/\eta = (1 - \frac{\phi}{\phi_c})^{-2}$ (Maron-Pierce)
- $\eta_s/\eta = (1 + \frac{\frac{5}{4}\phi}{1 - \frac{\phi}{\phi_c}})^2$ (Eilers)

Measuring suspension viscosity

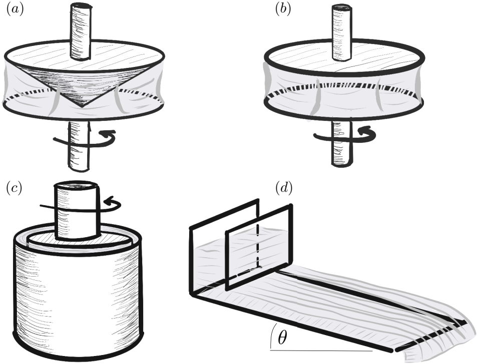

(a) Cone-and-plate rotational rheometer: $\eta = 3\alpha T/2\pi R^3\Omega$; *(b) Parallel-plate rotational rheometer*: $\eta = 2Th/\Omega\pi R^4$; *(c) Couette rotational rheometer*: $\eta = T(R_c - R_b)/\pi L\Omega(R_c + R_b)R_b^2$; *(d) Inclined plane rheometer*: $\eta = \rho g h^2 \sin\theta/2u_s$

Relative viscosity of suspensions $\eta_s(\phi)$

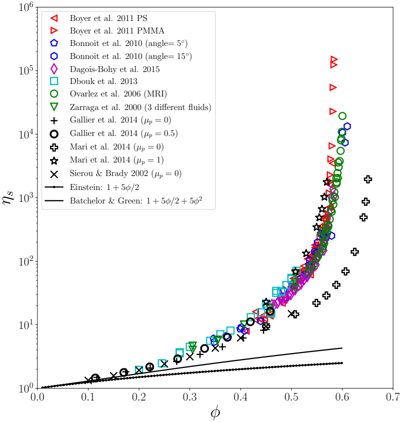

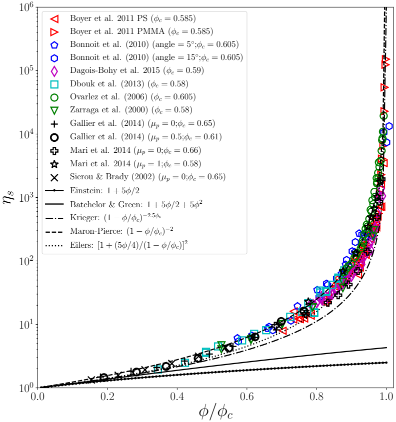

Divergence as $(\phi - \phi_c)^{-2}$ when $\phi \to \phi_c$ with $\phi_c \approx 0.54 - 0.62 < \phi_{crp} \approx 0.64$ $\therefore$ frictional spheres!
Shear-jamming fraction varies depending on size distribution and surface interactions (friction)

Normal stresses in suspensions

Normal stress differences

- $N_1 = \Sigma_{11} - \Sigma_{22}$
- $N_2 = \Sigma_{22} - \Sigma_{33}$

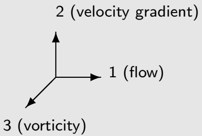

Normal stress differences in non-Brownian suspensions

- $N_1, N_2 \propto \eta_f \dot{\gamma}$ linear in $\dot{\gamma} = \sqrt{2\,\mathbf{E} : \mathbf{E}}$
- $N_i/\tau = O(1) \equiv \alpha_i(\phi)$ same divergence as $\phi \to \phi_c$
- $|N_2| \gg |N_1|$
- N_2 negative but sign of N_1 more elusive!

Gadala-Maria 1979, Zarraga, Hill & Leighton 2000; Singh & Nott 2003; Couturier, Boyer, Pouliquen & Guazzelli 2011; Dai, Bertevas & Tanner 2013; Dbouk, Lobry & Lemaire 2013; Gamonpilas, Morris & Denn 2016
Sierou & Brady 2002; Gallier, Lemaire, Peters & Lobry 2014; Gallier, Lemaire, Lobry & Peters 2016

Origin of normal stress differences in suspensions

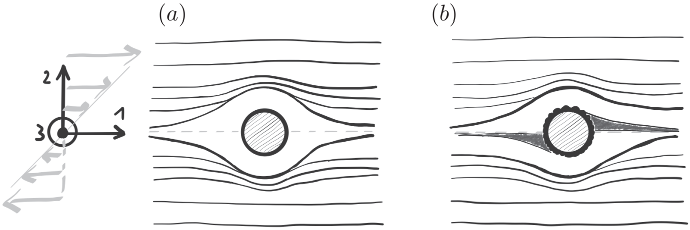

Pair interaction between particles under simple shear

Surface roughness or repulsive force:
→ irreversible and asymmetric collisions
Arp & Mason J. Colloid Interface Sci. 1977; Davis PoF 1992
→ non-isotropic normal stresses
Brady & Morris JFM 1997; Wilson JFM 2005

Breakdown of fore-aft symmetry (depletion in extensional quadrants)

Measuring normal stress differences

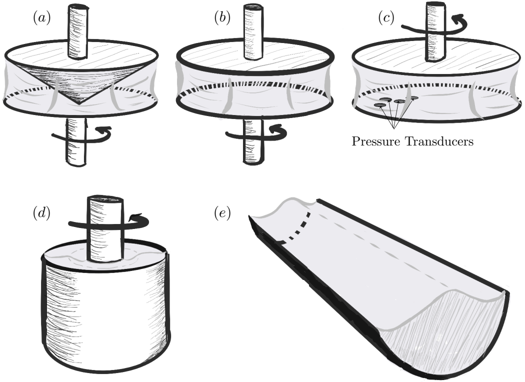

(a) Cone-and-plate rotational rheometer: N_1; *(b) Parallel-plate rotational rheometer*: $N_1 - N_2$; *(c) Parallel-plate rheometer with differential pressure transducers fitted flush against the lower plate surface*: $N_2 + N_1/2$ and $N_1 + N_2$; *(d) Weissenberg, or rotating rod, flow*: $N_2 + N_1/2$; *(e) Tilted-trough flow*: N_2

Evidence of these normal stress differences

Free-surface deflection in rotating-rod and tilted-trough flows

Rotating-rod flow: anti-Weissenberg or rod dipping effect

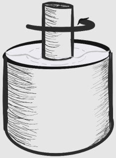

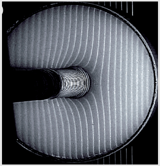

$\rightarrow$ measurement of $N_2 + N_1/2$

Boyer, Pouliquen & Guazzelli JFM 2011

Tilted-trough flow: bulging of the free surface

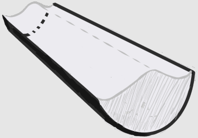

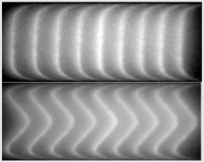

$\rightarrow$ measurement of N_2

Couturier, Boyer, Pouliquen & Guazzelli JFM 2011

Normal stress differences can be described as a tension in the vortex line!

Hinch JFM Focus in Fluids 2011

Normal stress coefficients $\alpha_1 = N_1/\tau$ and $\alpha_2 = N_2/\tau$

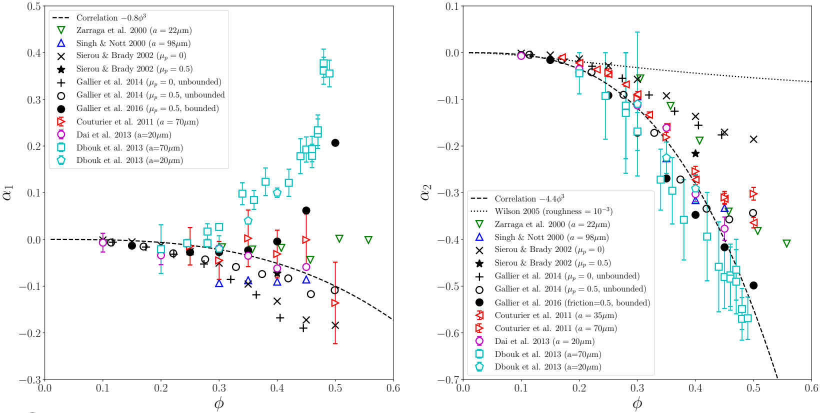

- First normal stress coefficient $\alpha_1(\phi)$ small but sign elusive: negative, positive, or null!
- Second normal stress coefficient $\alpha_2(\phi)$ negative and magnitude increases with increasing ϕ
- Simulations show importance of friction and effect of confinement/walls

Normal stress coefficients $\alpha_1 = N_1/\tau$ and $\alpha_2 = N_2/\tau$

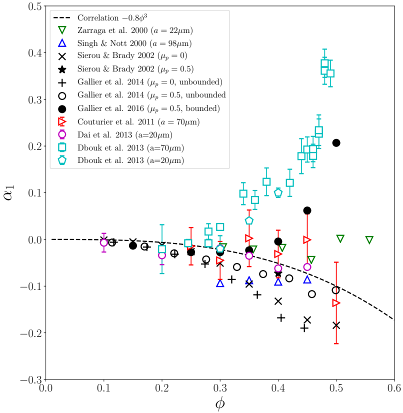

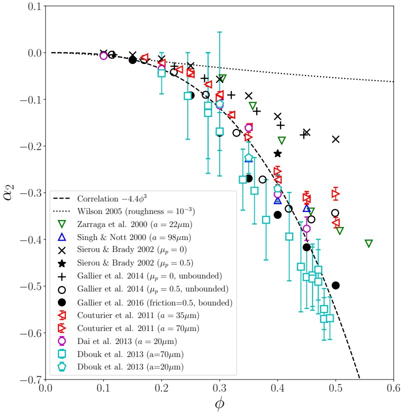

- N_2 large and negative because of lack of serious repulsion in the vorticity direction (most of the repulsive collisions between spheres happen in the plane of shear)

Normal stress coefficients $\alpha_1 = N_1/\tau$ and $\alpha_2 = N_2/\tau$

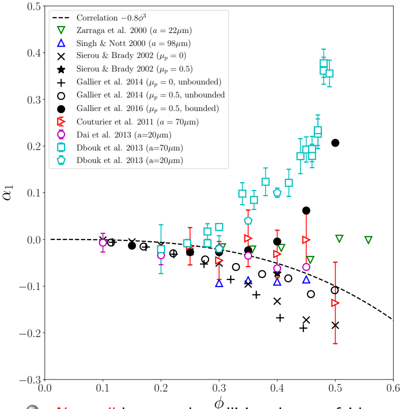

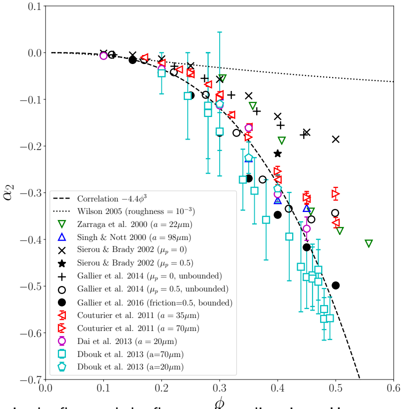

- N_1 small because the collisions happen fairly equally in the flow and the flow-gradient directions. However, the flow-induced microstructure of the frictional spheres can explain the sign of N_1: (i) in the bulk, the deficit in hydrodynamic interactions in the extensional region leads to a negative sign and (ii) near a wall, the particle layering results in a decrease of contact stresses (enhanced by friction) and thus positive sign.

1. The suspension as a single effective fluid
   - Suspension viscosity
   - Non-Newtonian behavior: normal stresses
2. Beyond the single-fluid view: two-phase flow
   - Particle pressure
   - Two-phase flow: shear-induced migration
3. An alternative frictional approach
4. Microscopic origin of the rheology
   - Microstructure
   - Irreversibility – role of contacts
5. Approaching jamming
   - Origin of the jamming transition
   - Influence of particle roughness and shape
6. Towards more complex suspensions

Beyond the single-fluid view: two-phase flow

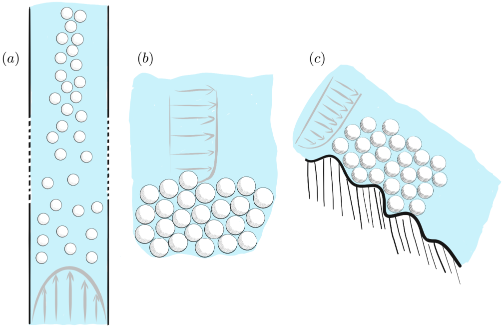

Examples of two-phase suspension flows: (a) Shear-induced migration of neutrally-buoyant spheres in a pressure-driven Poiseuille flow in a tube; (b) Erosion of sedimented particles under the action of viscous fluid shearing flows; (c) Submarine avalanches forced by the fluid shear stress

Physical illustration of the particle pressure

Suspension mixture incompressible but not particle phase!

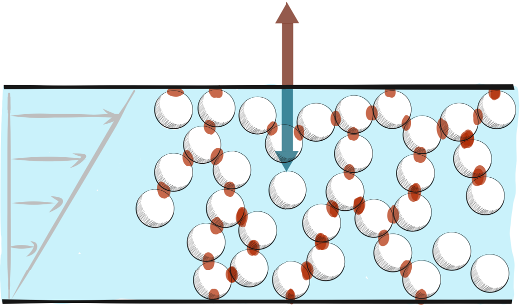

In a sheared suspension of particles, the collisions between the particles and between the particles and the walls creates a force against the wall. This leads to a 'particle pressure', i.e. a pressure coming for the particulate phase. Since the total pressure created by suspension mixture (particles plus fluid) is constant because of the incompressibility of the suspension, this 'particle pressure' is balanced by a pressure coming from the fluid phase.

Analogy with osmotic pressure

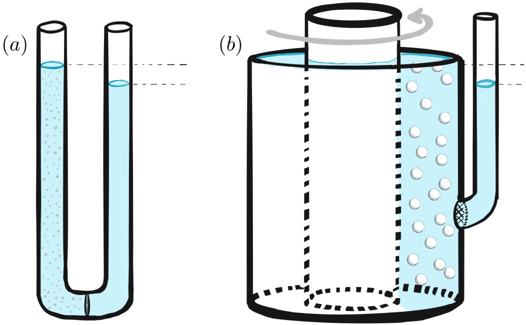

(a) Osmotic U tube: The solution is separated from the pure solvent (or a lower concentration solution) by a semi-permeable membrane permitting the flow of the solvent but restricting the solute to the solution side. Osmotic pressure is associated with the solvent flow into the solution and is measured by a reduced pressure in the solvent
(b) Analogical experiment using a Couette device: When the suspension is sheared, the liquid is sucked from the tube through the grid. The liquid suction pressure is a way of evidencing and measuring the particle pressure

Deboeuf, Gauthier, Martin, Yurkovetsky & Morris PRL 2009

Methods for measuring particle normal stresses

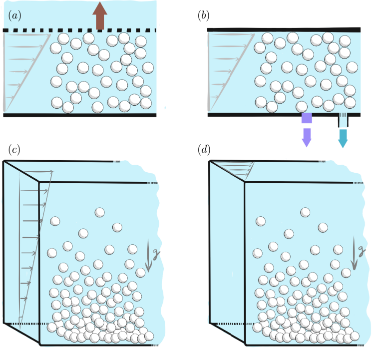

(a) Grid pressure measurement; (b) Pore pressure measurement; Viscous resuspension: Measurement can be conducted (c) in the plane of shear or (d) in the plane perpendicular to the plane of shear (i.e. in the vorticity direction)

Particle pressure

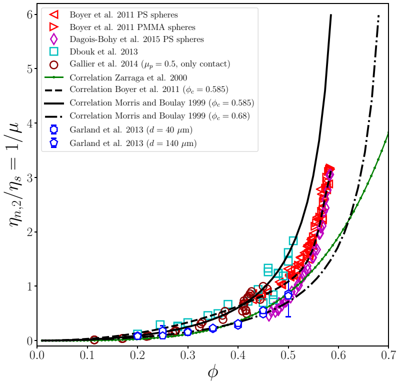

Particle pressure in the gradient direction

Viscous scaling

$-\sigma^p_{22} = \eta_{n,2}\eta_f|\dot{\gamma}|$
(independent of the sign of the shear rate)

Normal viscosity: $\eta_{n,2}(\phi)$

Same divergence as $\eta_s(\phi)$

Effective friction coefficient: $-\sigma^p_{22}/\tau = \eta_{n,2}/\eta_s = 1/\mu$

- $\eta_{n,2}/\eta_s \rightarrow$ constant value (≈ 3.3, i.e. $\mu \approx 0.3$) when $\phi \rightarrow \phi_c (\approx 0.58 - 0.59)$
- $\eta_{n,2}/\eta_s \rightarrow 0$ when $\phi \rightarrow 0 \quad \therefore \eta_{n,2} \rightarrow 0$

Particle normal stresses

General tensorial form

$$-\eta_f|\dot{\gamma}| \begin{pmatrix} \eta_{n,1}(\phi) & 0 & 0 \\ 0 & \eta_{n,2}(\phi) & 0 \\ 0 & 0 & \eta_{n,3}(\phi) \end{pmatrix}$$

Simplified form (similar ϕ-dependence in all the directions) (Morris & Boulay JoR 1999)

$$-\eta_n(\phi)\,\eta_f|\dot{\gamma}| \begin{pmatrix} 1 & 0 & 0 \\ 0 & \lambda_2 & 0 \\ 0 & 0 & \lambda_3 \end{pmatrix}$$

with

$$\eta_n(\phi) = \kappa \left(\frac{\phi_c - \phi}{\phi} \right)^{-2}$$

with $\kappa \approx 0.75$, $\lambda_2 \approx 0.8$, and $\lambda_3 \approx 0.5$ (Morris & Boulay JoR 1999)
with $\kappa \approx 1$, $\lambda_2 \approx 0.95$, and $\lambda_3 \approx 0.6$ (Boyer, Guazzelli & Pouliquen PRL 2011)

Observation of shear-induced migration

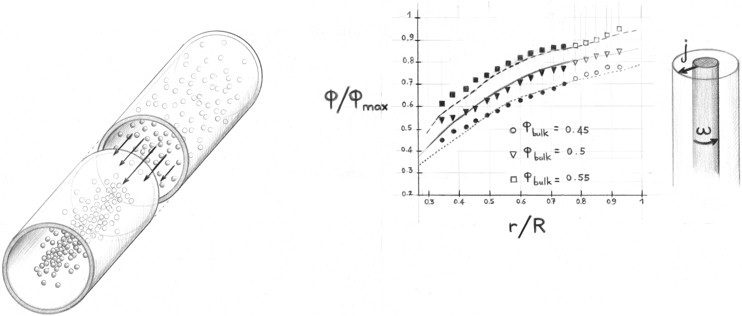

Particle migration from regions of high to low shear rate

Karnis, Goldsmith & Mason J. Colloid Interface Sci. 1966, Leighton & Acrivos JFM 1986 ...

Shear-induced migration in pipe flow

Particle migration toward the center of the pipe

Snook, Butler & Guazzelli JFM 2016

Discrete-particle simulations: Stokesian Dynamics

Two-phase modeling of suspensions

Continuum two-phase modeling

- to assume that the interstitial fluid and the particles are two intertwined continuous phases
- to derive the governing equations that describe the system in an average sense for each phase

Different ways of performing the averaging process

- local space averaging over regions smaller than the macroscopic length scale but larger than the particle size
- ensemble averaging at each point of space over 'macroscopically equivalent' systems

Averaged equations

- for the two phases and for the whole suspension but only two sets needed
- closure problem: need for some constitutive relations

see e.g. Jackson Chem. Engng Sci 1997, Nott, Guazzelli & Pouliquen PoF 2011

The suspension balance model: migration equation

Balance equations for the particle phase

$$\frac{\partial \phi}{\partial t} + \nabla \cdot (\phi \mathbf{u}^p) = 0$$

$$\nabla \cdot \boldsymbol{\sigma}^p + n\langle \mathbf{f}^h \rangle^p_{\rm drag} + \phi(\rho_p - \rho_f)\mathbf{g} = 0$$

with

$$n\langle \mathbf{f}^h \rangle^p_{\rm drag} = -\frac{9\eta_f}{2a^2}\frac{\phi}{f(\phi)}(\mathbf{u}^\mathbf{p} - \mathbf{U}) \quad \text{with} \quad f(\phi) = (1-\phi)^n \quad \text{Richardson \& Zaki 1954}$$

Incompressibility of the suspension

$$\nabla \cdot \mathbf{U} = 0$$

with volume average velocity: $\mathbf{U} = \phi\, \mathbf{u}^p + (1-\phi)\, \mathbf{u}^f$

Migration equation for neutrally buoyant particles, $\rho = \rho_p = \rho_f$

$$\frac{\partial \phi}{\partial t} + \mathbf{U} \cdot \nabla \phi = -\nabla \cdot \phi(\mathbf{u}^\mathbf{p} - \mathbf{U}) = -\frac{2a^2}{9\eta}\nabla \cdot [f(\phi)\nabla \cdot \boldsymbol{\sigma}^p]$$

Nott & Brady JFM 1994; Morris & Boulay JoR 1999; Lhuillier PoF 2009; Nott, Guazzelli & Pouliquen PoF 2011

Pressure-driven flow in a 2D channel

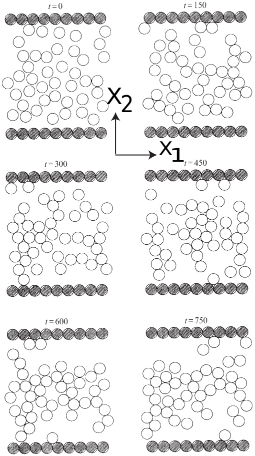

Nott & Brady JFM 1994

Migration equation

$$\frac{\partial \phi}{\partial t} = -\frac{a^2}{9\eta_f}\frac{\partial}{\partial x_2}\left[f(\phi)\frac{\partial \sigma^p_{22}}{\partial x_2}\right]$$

Momentum equation for the whole suspension along x_1

$$G = \frac{\partial \tau}{\partial x_2} = \frac{\partial\left[\eta_s(\phi)\eta_f\dot{\gamma}\right]}{\partial x_2}$$

Steady fully developed flow

- Particle pressure constant across the channel

$$-\frac{\partial \sigma^p_{22}}{\partial x_2} = \frac{\partial[\eta_{n,2}(\phi)\,|\dot{\gamma}(x_2)|]}{\partial x_2} = 0$$

- Where the shear rate is low, the concentration is high and vice versa and the particles must have migrated to the center

Evolution of the concentration profiles in a 2D channel

Comparisons SBM, simulations, and experiments

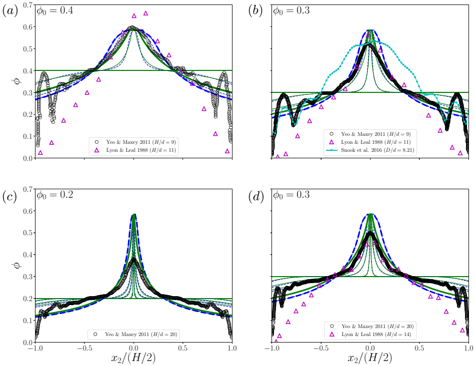

Agreement at large ϕ but some discrepancies at smaller ϕ and for the dynamics

An alternative description: pressure-imposed rheology

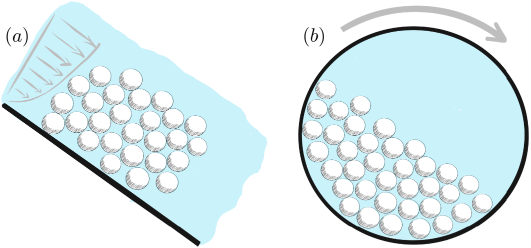

Examples of gravity-driven flows of suspensions of negatively-buoyant particles. Flows of immersed heavy particles (a) down an inclined plane and (b) in a tumbler. In both cases, the driving force is gravity; it controls the level of stress experienced by the particle phase whereas the volume fraction is free to adjust to the flow condition

Granular rheology

Friction and dilatancy laws in the granular-liquid regime

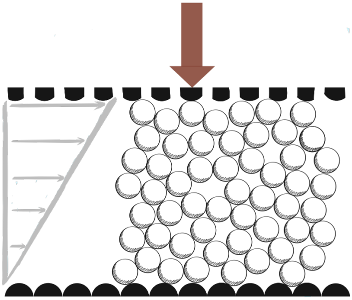

GDR MiDi 2004; da Cruz, Emam, Prochnow, Roux & Chevoir 2005; Lois, Lemaitre & Carlson 2005

Inertial number

$$I = \frac{\dot{\gamma} d}{\sqrt{P/\rho_p}}$$

Pressure on the top plate P and shear rate $\dot{\gamma}$ imposed:

$$\begin{aligned} \tau/P &= \mu(I) \\ \phi &= \phi(I) \end{aligned}$$

The shear stress is proportional to the pressure, with the effective friction coefficient μ and the volume fraction ϕ being functions of I

Forterre & Pouliquen ARFM 2008

Volume-imposed versus pressure-imposed rheometry

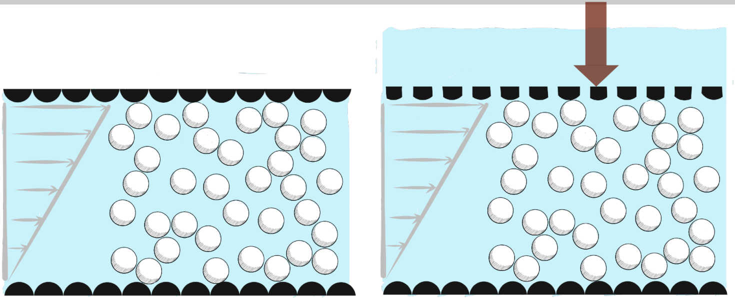

Volume-imposed rheometry: $P, \tau, \dot{\gamma}, \phi, \eta_f$

- $\tau = \eta_s(\phi)\,\eta_f \dot{\gamma}$
- $P = \eta_n(\phi)\,\eta_f \dot{\gamma}$

Viscous scaling of the stresses

Pressure-imposed rheometry: $\phi, \tau, \dot{\gamma}, P(\equiv -\sigma^p_{22}), \eta_f$

- $\tau / P = \mu(J)$
- $\phi = \phi(J)$

$J = \eta_f \dot{\gamma}/P$ **viscous** dimensionless shear rate

Dimensionless shear rate

Inertial dimensionless number
$I = d\dot{\gamma}/\sqrt{P/\rho_p}$

Ratio between two time scales

1. macroscopic time scale linked to the mean deformation: $1/\dot{\gamma}$
2. inertial microscopic time of rearrangements: $d/\sqrt{P/\rho_p}$

GDR MiDi 2004; da Cruz, Emam, Prochnow, Roux & Chevoir 2005; Lois, Lemaitre & Carlson 2005

Viscous dimensionless number
$J = \eta_f \dot{\gamma}/P$

Ratio between two time scales

1. macroscopic time scale linked to the mean deformation: $1/\dot{\gamma}$
2. viscous microscopic time of rearrangements: η_f/P

Cassar, Nicolas & Pouliquen 2005; Boyer, Guazzelli & Pouliquen 2011

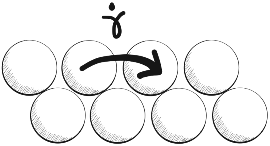

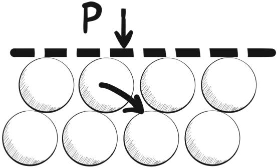

Pressure-imposed rheology of suspension

Alternative frictional view coming from the rheology of dry granular materials

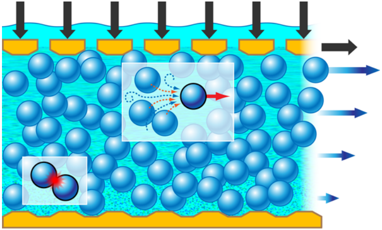

from a Viewpoint on Unifying Suspension and Granular Rheology Boyer, Guazzelli & Pouliquen PRL 2011 Physics 2011 (APS/Alan Stonebraker)

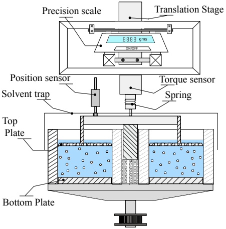

- Top porous plate enabling fluid to flow through it but not particles
- Simultaneous measurements of ϕ, $\dot{\gamma}$, τ, $P(\equiv -\sigma_{22}^{p}$ here)

- Measurements of the particle pressure P
- Examination of the rheology close to the jamming transition

Boyer, Guazzelli & Pouliquen PRL 2011

Dry granular versus immersed granular rheology

Inertial dry granular media: inertial dimensionless number $I = d\dot{\gamma}/\sqrt{P/\rho_p}$

$\mu(I)$ saturates at large I and $\phi_c - \phi \propto I$

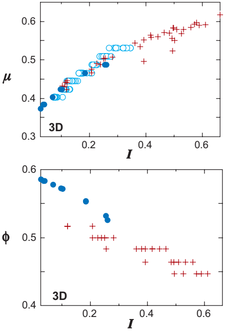

data (inclined-plane and annular shear geometry) collected in Forterre & Pouliquen ARFM 2008

Viscous Newtonian suspensions: viscous dimensionless number $J = \eta_f\dot{\gamma}/P$

$\mu(J)$ still increases at large J and $\phi_c - \phi \propto J^{1/2}$

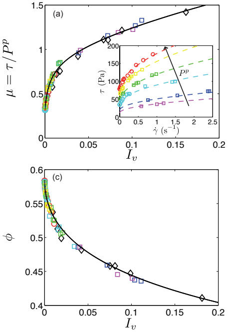

Boyer, Guazzelli & Pouliquen PRL 2011

Classical effective viscosity recovered from frictional view

Unifying suspension and granular rheology

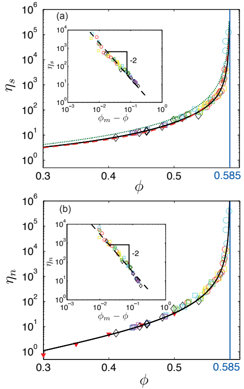

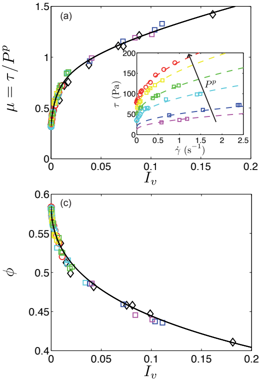

using $\eta_s = \mu/J$ and $\eta_n = 1/J$
from $\mu = \tau/P = \eta_s/\eta_n$ and $J = \eta_f\dot{\gamma}/P = 1/\eta_n$

The pair distribution function

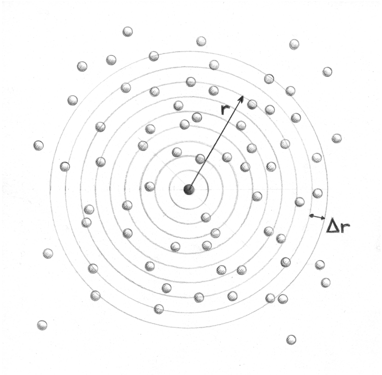

The pair distribution function provides the likelihood of finding a particle at position **r** with respect to a reference particle, relative to the likelihood of finding a particle at any position within the suspension without knowledge of any particle position

Measuring the pair distribution function

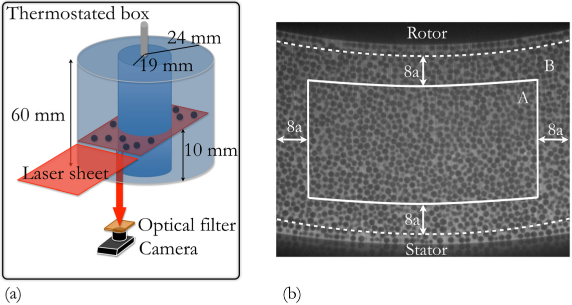

Density and index-matched suspension sheared in a wide-gap Couette rheometer

First experimental attempt: Parsi & Gadala-Maria JoR 1987
Recent experimental determinations: Blanc, Lemaire, Meunier & Peters JoR 2013

Experimental pair distribution function in the shear plane

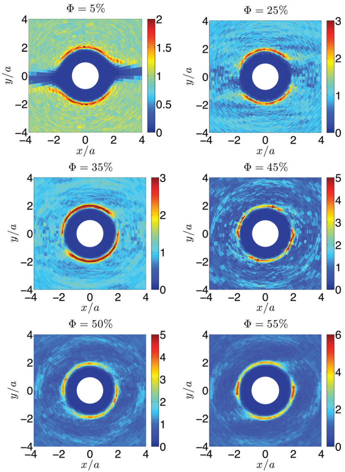

- For $\phi = 0.05$:
  - Fore-aft asymmetry due to particle surface roughness
  - depleted area + tail-like high particle concentration zone in the recession quadrant
- For all ϕ: strong pair correlation zone near $\rho/a = 2$ in the compressional quadrant + depleted zone in the extensional quadrant
- As the particle concentration increases, the depleted zone that is close to the velocity direction for $\phi = 0.05$ rotates toward the dilatation axis direction
- For $\phi > 0.45$: secondary depletion zone in the compressional quadrant + high pair correlation zone near the mean flow direction

Blanc, Lemaire, Meunier & Peters JoR 2013

Numerical pair distribution function in the shear plane

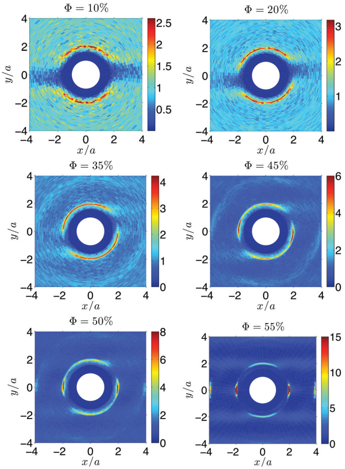

Same qualitative features with Stokesian Dynamics simulations in where repulsive forces between particles have been tuned to reproduce the particle roughness effects

Blanc, Lemaire, Meunier & Peters JoR 2013

Microstructure

Pair distribution of suspensions of non-Brownian rough spheres

- Fore-and-aft asymmetric with a strong pair correlation zone at contact in the approach side of the reference particle and a depletion of pairs in the receding side
- At low particle volume fraction, the depleted area is close to the velocity direction and is tilted as the particle concentration is increased
- At very high concentrations, new features: a secondary depleted area in the compressional quadrant and a probability peak in the velocity direction

Microstructure and non-Newtonian rheology

The essential point is that the microstructure loses isotropy, establishing a preferred direction for finding the near-contact pairs that control the observed rheology of concentrated suspensions. This anisotropy leads to normal stress differences in shear flow and the shear-induced migration phenomenon.

Evidence of a shear-induced anisotropic microstructure

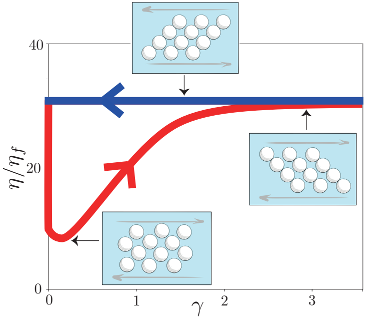

Gadala-Maria & Acrivos JoR 1980

Blanc, Peters & Lemaire JoR 2011

Steady shearing of a suspension

The particles organize into a microstructure where the contacts are predominantly oriented along the compressional directions

Shear reversal (at large ϕ)

The viscosity exhibits a sudden drop, corresponding to the loss of the contacts, and then increases to return to its steady value as the contact arrangement slowly rebuilds in the new compressional zones

Irreversibility of pair trajectories in simple shear

Crucial role of surface roughness near contact of the pair

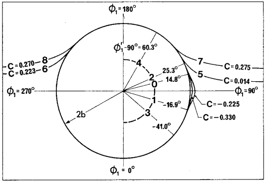

Fig. 8. Polar diagram of the trajectories listed in Table V for flow reversals 0 to 8. Also shown are the angles $\phi_1{}^r - 90°$ at which the flow was reversed and when the spheres were close together. Initially the spheres moved along closed trajectories ($C = -0.33$) which did not change significantly until after the third flow reversal (when C increased to -0.23). After the fourth reversal the trajectories became open ($C = +0.01$) and on the fifth reversal the spheres were allowed to pass each other at $\phi_1 = 0, 180°$ resulting in a further increase in C, which became effectively constant after the sixth reversal when $C \simeq 0.27$. The trajectories were calculated from [1] and [2], knowing B and C obtained experimentally from analysis of cinefilms taken along the x_1 and x_2 axes.

Arp & Masson J. Colloid Interface Sci. 1977

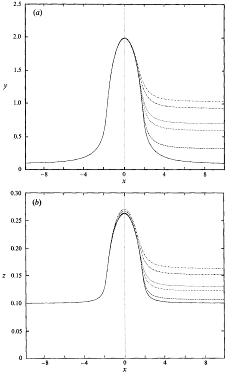

Figure 1. The effect of roughness on particle trajectories, (a) in the (x, y)-plane and (b) in the (x, z)-plane. The initial conditions are $x = -10$ and $y = z = 0.1$. The different curves correspond to different values of the roughness: ———, $\epsilon = 0$; – – – – – –, $\epsilon = 10^{-4}$; – – – – – –, $\epsilon = 5 \times 10^{-4}$; ----------, $\epsilon = 10^{-3}$; –·–·–·–, $\epsilon = 5 \times 10^{-3}$ and –·–·–·–, $\epsilon = 10^{-2}$.

Da Cunha & Hinch JFM 1996

Signature of the pair trajectories of rough spheres in the shear-induced microstructure

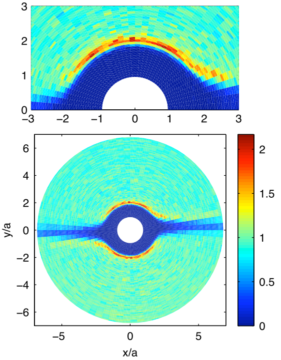

Pair distribution function
Blanc, Peters & Lemaire PRL 2011

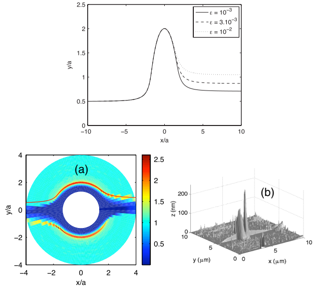

Pair distribution function computed from pair trajectories of rough spheres

Irreversibility of particle trajectories in periodic shear

Evidence that particles experience solid-solid contacts

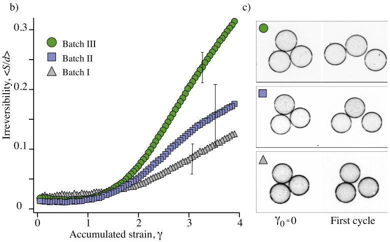

Irreversibility amplitude increases with increasing roughness
Pham, Metzger & Butler PoF 2015

Irreversibility in non-Brownian particle suspensions

Oscillatory Couette flow with a particle suspension

Pine, Gollub, Brady & Leshansky Nature 2005; Bricker & Butler JoR 2006,2007; Corté, Chaikin, Gollub & Pine Nature Physics 2008
and also: Memory impairment in flowing suspensions. Okagawa & Mason Science 1973; Okagawa, Ennis & Mason Can. J. Chem. 1978

Any small source of irreversibility in a physical system (e.g., surface roughness or repulsive forces, particles deformability, or inertia) can cause a loss of memory

Onset of irreversibility for large strain amplitudes

Particles observed stroboscopically
Strain amplitude = 1.0 (left) and 2.5 (right)

Pine, Gollub, Brady & Leshansky Nature 2005

Anisotropic random walk and shear-induced diffusion

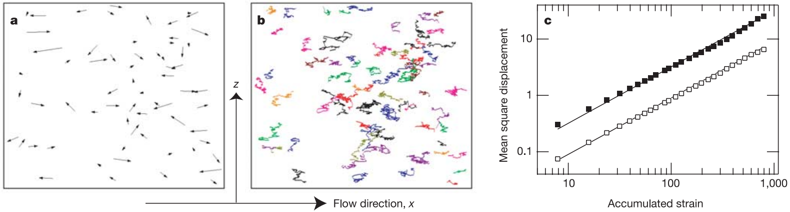

Figure 1 | Particle displacements and trajectories. a, Particle displacements in the x–z plane after one full cycle in a sheared suspension above the onset of irreversibility, amplified by a factor of 6 for clarity (volume fraction $\phi = 0.30$, strain amplitude $\gamma_0 = 2$). **b**, Some of the chaotic particle trajectories. **c**, Mean square particle displacements $\langle \Delta x^2 \rangle$ and $\langle \Delta z^2 \rangle$ after n full cycles as a function of the accumulated strain $\gamma = 4\gamma_0 n$ for $\phi = 0.40$ and $\gamma = 2.0$. The filled and open squares are the mean square displacements $\langle x^2 \rangle$ and $\langle z^2 \rangle$, respectively, obtained by averaging over particle trajectories such as those displayed in **b**; the solid lines through the data are least squares fits from which the diffusivities are determined. The fluctuations are anisotropic, growing more quickly along the flow direction (x) than along the axial direction (z). Experimental details: the diameter of the inner cylinder of the Couette cell is 50 mm and the gap between the (concentric) cylinders is 2.5 mm; thus, a strain of 1 corresponds to an angular displacement of the inner cylinder of 5.7°. The PMMA particles have surface irregularities of only 2 nm, as measured by AFM. The fluid viscosity is 3 Pa s, about 3,000 times that of water. The suspension floats on a layer of mercury to eliminate end effects. The fractional accuracy of the phase at which the camera and frame grabber are triggered is typically better than 0.001, but the final results are not very sensitive to this quantity. We sample particle positions near the instant of maximum particle velocity. The particle displacements in the x and z directions after each full cycle are denoted by Δx and Δz, respectively.

Pine, Gollub, Brady & Leshansky Nature 2005

Threshold of irreversibility in an oscillatory shearing flow

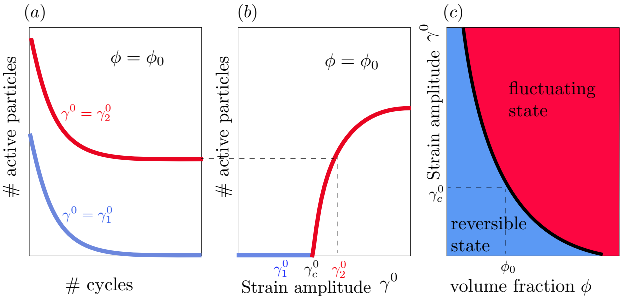

Dynamical phase transition between a fluctuating irreversible steady state (wherein a finite fraction of active particles experience random diffusive motions) and an absorbing reversible state (wherein the particles avoid each other)

Pine, Gollub, Brady & Leshansky Nature 2005; Corté, Chaikin, Gollub & Pine Nat. Phys. 2008

1. The suspension as a single effective fluid
   - Suspension viscosity
   - Non-Newtonian behavior: normal stresses
2. Beyond the single-fluid view: two-phase flow
   - Particle pressure
   - Two-phase flow: shear-induced migration
3. An alternative frictional approach
4. Microscopic origin of the rheology
   - Microstructure
   - Irreversibility – role of contacts
5. Approaching jamming
   - Origin of the jamming transition
   - Influence of particle roughness and shape
6. Towards more complex suspensions

Increased role of contact with increasing concentration

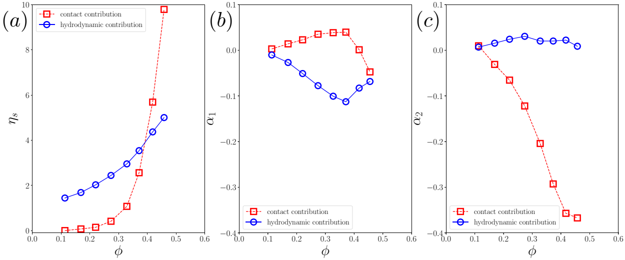

Relative contribution of the frictional contact (red square) and of the hydrodynamic (blue circle) stresses to the (a) viscosity, and the (b) first and (b) second normal stress differences as a function of the volume fraction, ϕ

Gallier, Lemaire, Peters & Lobry JFM 2014

Extended network of contacts close to jamming

Perturbations around the jammed state to predict the singular behaviors

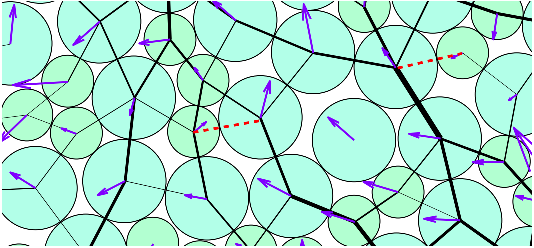

Illustration of solid destabilization: several weak contacts (red dashed lines) are opened. This induces a space of extended, disordered floppy modes, one of which is shown (arrows). Line thickness indicates force magnitude in the original, stable solid.

DeGiuli, Düring, Lerner & Wyart PRE 2015

Amplification of the rheological properties caused by the addition of particles

Local shear rate: $\dot{\gamma}_{local}$

- linked to the magnitude of shear rate experienced by the interstitial fluid between the particles (e.g. the standard deviation of the modulus of the shear rate)
- larger than the macroscopic shear rate, $\dot{\gamma}$, imposed to the whole suspension mixture

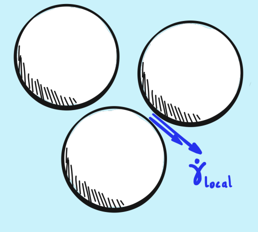

Amplification factor: the lever function, $\mathcal{L}(\phi)$, depending solely on ϕ

$$\dot{\gamma}_{local} = \mathcal{L}(\phi)\,\dot{\gamma}$$

Lever function diverges when approaching ϕ_c and is directly related to the density of floppy modes, i. e. related to the 'extended' open contacts leading to a spatially extended response in the system

Amplification of the viscosity related to the lever function

Homogenization approach

Energy dissipated per unit of time and volume, $\mathcal{P}$

- whole suspension mixture: $\mathcal{P} = \eta_s(\phi)\,\eta_f\dot{\gamma}^2$
- assuming that the dissipation mainly occurs in the interstitial fluid and not at the contact between the particles, exact in the limit of **frictionless particles**: $\mathcal{P} = (1-\phi)\eta_f\dot{\gamma}^2_{local}$

Relation between the relative shear viscosity and the lever function

$$\eta_s(\phi) = \frac{(1-\phi)\dot{\gamma}^2_{local}}{\dot{\gamma}^2} = (1-\phi)\mathcal{L}(\phi)^2$$

Scaling description of rheological properties near jamming

- **For frictionless particles:** $\eta_s(\phi) \sim (\phi_c - \phi)^{-2.83}$
- **For frictional particles: energy also dissipated by sliding at frictional contacts**

Chateau, Ovarlez & Trung JoR 2008; DeGiuli, Düring, Lerner & Wyart PRE 2015

Influence of interparticle friction on rheological properties

Inertial granular flows

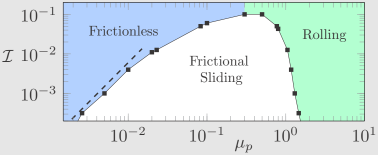

In the frictionless and rolling regimes, most energy is dissipated by inelastic collisions, while in the frictional sliding regime energy dissipation is dominated by sliding
DeGiuli, McElwaine & Wyart PRE 2016

Viscous suspension flows

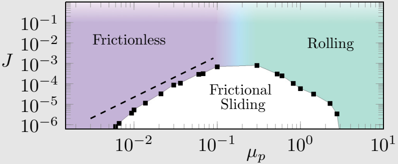

In the frictionless and rolling regimes, the dominant source of dissipation is viscous drag, whereas in the frictional sliding regime, dissipation is dominated by sliding friction
Trulsson, DeGiuli & Wyart PRE 2017

Impact of interparticle friction, and in particular of surface roughness, on the rheological properties of these particulate systems close to the jamming transition

Slightly and highly roughened spheres

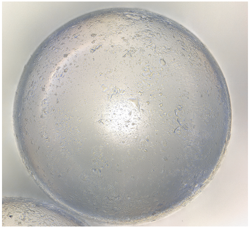

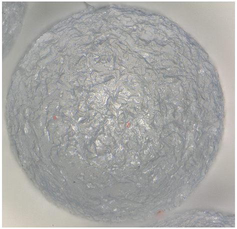

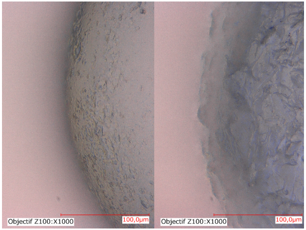

Slightly roughened (SR) and highly roughened (HR) spheres

	R_a[a] (μm)	R_q[b] (μm)	R_z[c] (μm)	μ_{sf}	μ_{rf}	d (μm)
SR	0.287 ± 0.008	0.387 ± 0.008	2.073 ± 0.008	0.23 ± 0.03	0.004 ± 0.001	580 ± 20
HR	1.896 ± 0.008	2.410 ± 0.008	9.808 ± 0.008	0.37 ± 0.03	0.007 ± 0.001	540 ± 20

[a] average roughness

[b] standard deviation

[c] ten-point mean roughness

Rheological data for the immersed and dry spheres

μ and ϕ versus $J = \frac{\eta_f \dot{\gamma}}{P}$ (immersed case) and $I = d\dot{\gamma}\sqrt{\frac{\rho_p}{P}}$ (dry case)

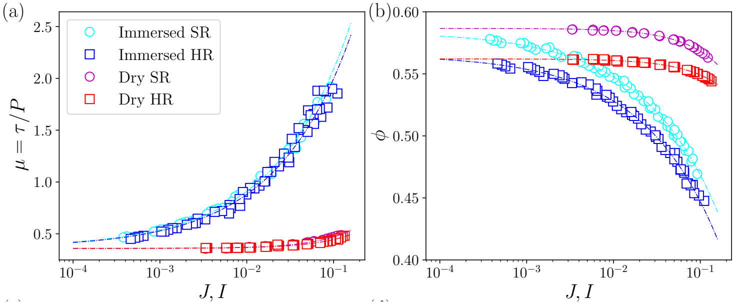

- μ unchanged while ϕ shifted toward lower values of ϕ when increasing particle roughness
- Critical values for the effective friction coefficient and the volume fraction:
  - $\mu_c \approx 0.36$ similar in the immersed and dry cases and not affected by particle roughness
  - ϕ_c similar in the immersed and dry cases but decreasing with increasing roughness: $\phi_c^{SR} \approx 0.585$ whereas $\phi_c^{HR} \approx 0.564$

Rheological data for the viscous (immersed) spheres

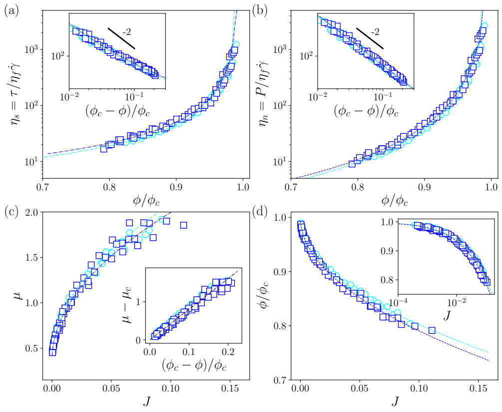

Tapia, Pouliquen & Guazzelli PRF 2019

Classical effective viscosity recovered from frictional view

$\mu = \tau/P = \eta_s/\eta_n$
$J = \eta_f\dot{\gamma}/P = 1/\eta_n$

$\therefore$

$\eta_s(\phi) = \mu(\phi)/J(\phi) = \mu(\phi)\eta_n(\phi)$
$\eta_n(\phi) = 1/J(\phi)$

Rescaling by ϕ_c

Complete collapse of all the data for both the SR and HR spheres

Asymptotic behaviors in the vicinity of the jamming transition

μ and $\phi \propto \sqrt{J}$
η_s and η_n diverge as $(1-\phi/\phi_c)^{-2}$

Rheology of rigid fiber suspensions

The different regimes of fiber suspensions

The dilute ($n \ll 1/L^3$), semi-dilute ($1/L^3 \lesssim n \ll 1/L^2 d$), concentrated ($n \gtrsim 1/L^2 d$) regimes and ordered nematic state ($n \gg 1/L^2 d$)

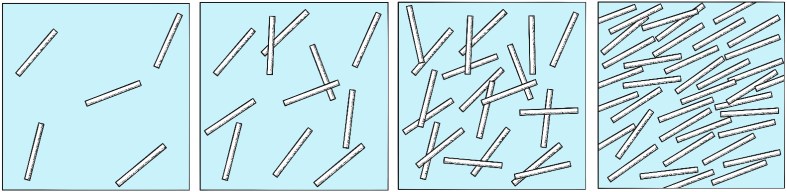

Rheology of viscous Newtonian fluids containing rigid fibers relatively unexplored

- Yield stresses and nonlinear scaling of τ with $\dot{\gamma}$ (shear-thinning)
  Ganani & Powell 1985; Powel 1991
- Rheological studies at relatively small ϕ ($\phi \lesssim 0.17$ for $A = 17 - 18$; $\phi \lesssim 0.23$ for $A = 9$)
  Bibbó 1985; Bounoua, Lemaire, Férec, Ausias & Kuzhir 2016

ϕ- and P-imposed rheometry of dense fiber suspensions

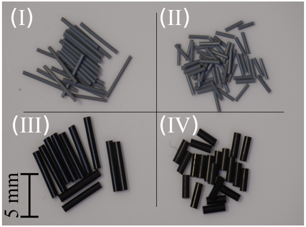

Rigid fibers with different aspect ratios

fiber label	Symbol	A
(I)	$\square$	14.5 ± 0.8
(II)	$\triangle$	6.3 ± 0.4
(III)	$\diamond$	7.2 ± 0.4
(IV)	$\bigcirc$	3.4 ± 0.3

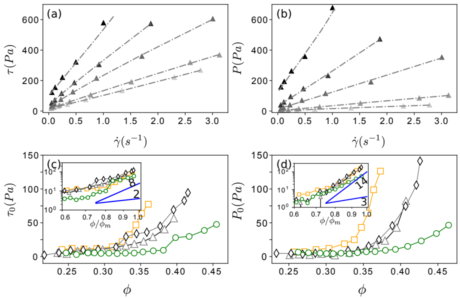

Viscous scaling: τ and P linear in $\dot{\gamma}$
But non-zero yield-stresses, τ_0 and P_0, at $\dot{\gamma} = 0$

- τ_0 and P_0 increase with ϕ, more sharply for higher A
- Origin of yield stresses still remains unknown!
  Adhesive forces? Transient jamming?

Rheological data after subtracting apparent yield-stresses

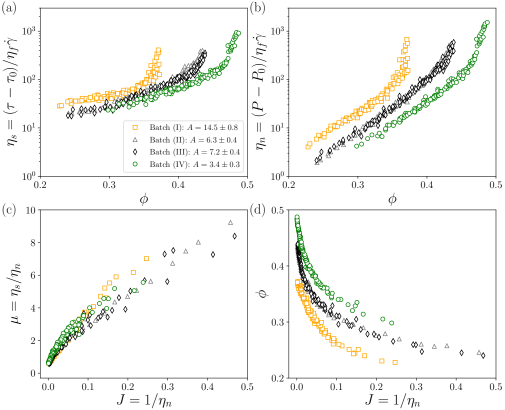

- η_s and η_n increase with ϕ and diverge at $\phi_c(A)$ with shift towards lower values of ϕ with increasing A
- ϕ decreasing function of J with shift towards lower values of ϕ with increasing A
- Good collapse of all data for $\mu(J)$
  $\therefore$ μ independent of A
- Data for batches (II) and (III), having similar A, collapse onto the same curve

Tapia, Shaikh, Butler, Pouliquen & Guazzelli JFM 2017

Critical values at jamming

Comparisons with:

- Experiments of Rahli, Tadrist & Blanc 1999 (■) on the dry packing of rigid fibers
- Simulations of Williams & Philipse 2003 (▲) for the maximum random packing of spherocylinders
- Data (★) obtained by Boyer, Guazzelli & Pouliquen 2011 for suspensions of spheres ($A = 1$)

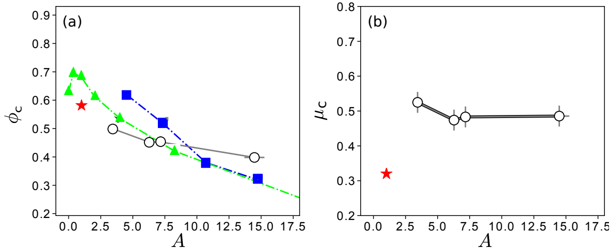

- ϕ_c decreases with increasing A such as for dry packing; organized structure for $A = 15$?
- $\mu_c \approx 0.47$ independent of A and larger than value for spheres (★)

Scaling at the jamming transition

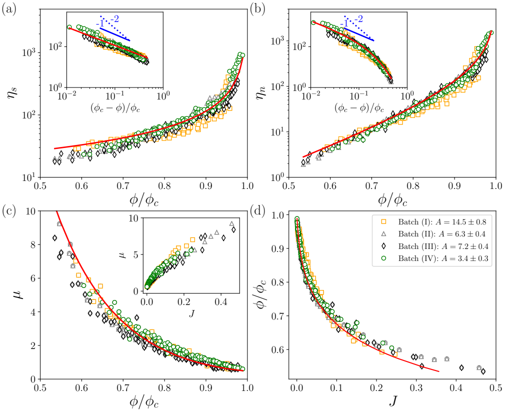

- Good collapse of all the data by rescaling by $\phi_c(A)$
- η_s and η_n diverge as $\sim (\phi_c - \phi)^{-1}$

Tapia, Shaikh, Butler, Pouliquen & Guazzelli JFM 2017

Towards more complex suspensions

- While hydrodynamic interactions between the particles are important in the dilute regime, they become of lesser significance when the concentration is increased, and direct particle contacts become dominant in the rheological response of concentrated suspensions.
- More open problems
  - Non-spherical particles (e.g. platelets . . .)
  - Colloidal interactions and nonlinear rheology: Shear-thickening (Wyart & Cates PRL 2014, Mari, Seto, Morris & Denn, JoR 2014)
  - Non-Newtonian fluids (Chateau, Ovarlez & Trung JoR 2008, Dagois-Bohy, Hormozi, Guazzelli & Pouliquen JFM 2015)
  - Inertial suspensions (Trulsson, Andreotti & Claudin PRL 2012, DeGiuli, Düring, Lerner & Wyart PRE 2015, Amarsid, Delenne, Mutabaruka, Monerie, Perales & Radjai PRE 2017)
  - Suspensions of polydisperse, deformable, active . . . particles
  - Suspensions at interfaces (Zhao, Oléron, Pelosse, Limat, Guazzelli & Roché PRR 2020)